JMEPEG (2021) 30:7752–7761
https://doi.org/10.1007/s11665-021-05939-2

1059-9495/$19.00

Experimental Investigation on Wire Electric Discharge Machining of Biodegradable AZ91 Mg Alloy

Levent Urtekin, Hacı Bekir Özerkan, Can Cogun, Asım Genc, Ziya Esen, and Fatih Bozkurt

Submitted: 24 January 2021 / Accepted: 22 May 2021 / Published online: 7 June 2021

The AZ91 magnesium alloy, used commonly as a biodegradable material in biomedical applications, is generally formed by conventional casting method (CCM) and high-pressure die casting method (HPDCM). The AZ91 alloys exhibit poor machinability with conventional chip removal methods since they degrade at elevated temperatures. In this study, the wire electric discharge machining (WEDM) was presented as a candidate process to machine the AZ91 alloy since no cutting stresses and plastic deformations were applied by the cutting tool to the part causing elevated temperatures. In this context, the WEDM machinability of the AZ91 alloy samples produced by cold chamber HPDCM and CCM at different process parameters, was experimentally investigated. The machining performance outputs (the machining current (I), the machining rate (MR), the average surface roughness (R_a), and surface topography) were found for the varying process parameters [pulse time (t_s), pulse-off time (t_{off}), dielectric flushing pressure (P_d), and wire speed (V_w)]. The present study revealed that the I and the MR were significantly dependent on the density, the porosity, and the micro structure of the samples, and the HPDCM samples gave the higher MR and the smoother surface than that of the CCM.

Keywords AZ91 alloy, machining current, machining rate, surface roughness, WEDM

1. Introduction

Magnesium (Mg) alloys are one of the lightest materials in industry and their excellent strength-to-weight ratio makes them desirable for many engineering applications such as in the automotive and aerospace industries. They have low melting point and high thermal conductivity. The AZ91 alloy with Mg-9Al-0.8Zn-0.2Mn (wt.%) configuration is the most frequently used Mg alloy in industry (90% of the overall Mg alloy applications) Ref 1-4. The alloy also preferred in biomedical applications as a biodegradable material since it degrades over time without leaving any foreign material when in contact with the body fluids. Therefore, no secondary surgery is needed for removal of the implant. Despite its good castability as well as favorable mechanical properties Ref 5, machinability of the alloy is poor Ref 1.

In recent years, there has been increased number of studies about AZ91 alloys, which aim strengthening and machining of the alloy. As well as the strengthening by grain size reduction and alloying, the strength of the alloy increases as a result of heat treatment operations like aging. Mathis et al. (Ref 6), for example, studied the effect of equal channel angular pressing (ECAP) at 270 °C on the microstructure and the mechanical properties of the AZ91 [Mg-9Al-1Zn-0.2Mn (wt.%)] samples, which were previously solution heat-treated for 18 h at 413 °C. It has been observed that besides grain refining, high temperature ECAP resulted in precipitation in the alloy. In addition, the shape of the $Mg_{17}Al_{12}$ precipitates also changed after several passes. The rod-shaped discontinuous precipitates were broken and after eight passes, the precipitates were observed to distribute homogeneously. The reduction in grain size and increased dislocation density enhanced the strength of the alloy as well below 100 °C. On the other hand, the ductility of the alloy increased when tested above 200 °C because of the recovery of the microstructure. On the other hand, in Türen (Ref 7) study, addition up to 0.5% Sn to the AZ91 resulted in an increase in the tensile strength and the yield strength, and a slight decrease in elongation without significant change in hardness.

In addition to usage of various strengthening techniques, Mg alloys should also be shaped into desired shape to be used for various applications without degradation of the alloy's mechanical properties. Among the various techniques, conventional chip removal processes are not suitable for obtaining intricate geometry especially for biomedical industry. On the other hand, unlike the conventional techniques, WEDM process does not damage the surface layer excessively; therefore, it became as an alternative manufacturing method for micro engineering and medical applications Ref 8. In biomedical applications, the surface condition of the material is crucial since it determines the interaction of the material with its surroundings in the body. Therefore, the effect of manufacturing process on the surface morphology should also be well defined in addition to investigations carried out about process variables to determine machining performance of the technique. Klocke et al. (Ref 9) examined the machining characteristics of the WE43 magnesium alloy using WEDM and found that WEDM process didn't damage the surface texture of the WE43 alloy surface as long as

Levent Urtekin, Mechanical Engineering Department, Faculty of Engineering and Architecture, Kırşehir Ahi Evran University, Kırşehir, Turkey; **Hacı Bekir Özerkan** and **Asım Genc**, Machinery and Metal Technology Department, Gazi University, Ankara, Turkey; **Can Cogun**, Mechatronics Engineering Department, Faculty of Engineering, Çankaya University, Ankara, Turkey; **Ziya Esen**, Materials Science and Engineering Department, Faculty of Engineering, Çankaya University, Ankara, Turkey; **Fatih Bozkurt**, Vocational School of Transportation, Eskişehir Technical University, Eskişehir, Turkey. Contact e-mail: levent.urtekin@ahievran.edu.tr.

suitable machining parameters were selected. Similarly, study of Mostafapor and Vahedi (Ref 10), which can be considered as the first comprehensive study on WEDM of magnesium alloys, revealed that the surface roughness of the machined alloy was acceptable despite the high cutting rate in comparison to hard materials. The study displayed that the process output parameters were influenced remarkably from the pulse time and machining current, while the number of WEDM passes was found to be insignificant. It was also stated that the material removal rate and the kerf width were considerably higher than those found in the hard materials.

The literature review revealed that there is no published study on the machinability characteristics of AZ91 alloy parts produced by different casting methods, which result in different microstructures. Therefore, in this study, the variation of machining performance outputs (I, MR, R_a and surface topography) of AZ91 alloy with varying WEDM process parameters (pulse time t_s, pulse interval t_{off}, dielectric flushing pressure P_d, and wire speed V_w) were investigated experimentally for AZ91 alloys produced by different techniques, namely conventional casting method (CCM) and cold chamber high-pressure die casting method (HPDCM). Additionally, the change of the surface topography and surface roughness of the alloys was investigated after machining.

2. Experimental Procedure

2.1 Material

The chemical composition of the AZ91 alloy used during casting by different methods is given in Table 1.

2.2 Fabrication of Cast Samples

The HPDCM and CCM samples to be WEDM machined were initially produced in the form of tensile test samples according to ASTM B557 M standard (Fig. 1). The CCM samples (labeled as Group 6 samples), which were received in as-cast condition, were prepared by turning of the 15 × 15 × 400 mm AZ91 alloy bar of stocks. On the other hand, the HPDCM samples (Groups 1-5) were cast initially using the MP100 Metal Press (1600 kN) cold chamber die casting machine. The temperatures of the fixed and the movable die were set to 175 °C and 225 °C, respectively (200 °C mean value). A 0.25% SF_6-N_2 (balance) protective gas mixture was used at a 600 L/h flow rate during casting of samples. Five different groups of casting parameters (Table 2) were employed during casting with HPDCM to examine the effect of the casting temperature, in-mold pressure and gate speed on the samples characteristics (density, porosities, cavities).

2.3 WEDM Parameters and Machining Experiments

The WEDM machine tool used in this study was Ultracut F1 (ELPULS 501). In this study, the set of machining parameters recommended by the control unit of the WEDM machine according to the specified material and size of the sample was named as "medium power level (MPL)." Moreover, two additional sets of parameters described by the authors of this study, one was lower and the other was higher than the MPL parameters (named as low-power level (LPL) and high-power level (HPL) parameters), were used in the present study to widen the experimental space (Table 3). The power level was increased by selecting longer pulse time t_s and shorter pulse-off time t_{off}. At HPL setting, a higher dielectric flushing pressure P_d was selected to provide effective removal of debris and ionized dielectric from the machining medium and faster cooling of the wire. The machining current I was continuously adjusted during the process by the control unit according to the thickness of the sample at the instant (more current passes when thickness increases). Each experiment was repeated three times and the average of the measurements were taken to ensure the reliability of the results.

In the experiments, the gage section of the tensile test samples, with 6±0.1 mm diameter and 60 mm gage length, was cut by WEDM in cross direction (at least three cuts). A 0.25-mm-diameter brass wire was used in the experiments. During the WEDM of the sample, maximum I was observed when the wire reached the full diameter of the sample. This value was recorded and used in the experiments. A 8 N wire tension was used throughout the experiments. The experiments were conducted for 4 and 6 m/min wire speeds (V_w) (Table 3). The variations of the machining performance outputs (I, MR, R_a and surface topographic characteristics) were examined for varying WEDM parameters (t_s, t_{off}, P_d, and V_w) for the samples produced by CCM and HPDCM.

Table 1. Chemical composition of AZ91 alloy ingots (wt.%)

Mg	Al	Cu	Ca	Zn	Mn
Balance	8.50	Max. 0.025	Max. 0.010	0.45	0.17

2.4 Characterization

The microstructural examination of as-cast samples prior to machining was conducted using light microscope (Eclipse LV150N, Nikon) through their polished and etched cross sections. The samples' surfaces were polished using Al2O3 (1 μm) suspensions after grinding and they were etched with 5% Nital solution. Scanning electron microscopy (SEM) was also performed using Hitachi Regulus 8230 to examine the surfaces of both as-cast and machined samples. The total porosity content of the as-cast samples was determined after determining the density of samples using Archimedes' Method at room temperature. A non-destructive technique was also used to monitor the presence of pores and cavities inside the as-cast sample according to ASTM E2869 standard and YXIon x-ray unit was used for this purpose. The x-ray tomography images of the samples were taken at 85 kW and 0.05 A. The average surface roughness (R_a) values were measured by Mitutoya Surftest SJ-210- Series 178 portable device. The electric resistivity of the samples before machining were measured by using VERIMET 4900C device with 0.3% accuracy.

3. Experimental Results

3.1 Microstructure and Surface Condition of As-cast Samples

Figure 2 displays the optical microscope images of the polished HPDCM (Group 1-5) and CCM samples. All of the HPDCM samples were observed to contain micro porosity

Figure 1. CCM sample prepared in the form of dog-bone tensile test sample according to ASTM B557 M standard

Table 2. HPDCM parameters

	HPDCM parameters		
Group	**Casting temperature, °C**	**In-mold pressure, bar**	**Gate speed, m/s**
1	660	1000	30
2	660	800	30
3	640	1200	60
4	680	1000	30
5	680	800	45

Table 3. WEDM parameters utilized in the present study

Parameter	LPL	MPL	HPL
Pulse-time t_s (μs)	110	117	123
Pulse-off time t_{off} (μs)	62	58	55
Flushing pressure P_d (bar)	8	10	12
Wire tension T (N)	8	8	8
Wire speed V_w (m/min)	4, 6	4, 6	4, 6

changing between ~ 2.5 and 5%; however, the CCM samples displayed very low amount of porosity of 0.3±0.2% (Table 4). The pores in the HPDCM samples were unhomogenusly distributed so that the images shown in Fig. 2 were taken from the regions where the pores were accumulated. Although there were no remarkable difference in porosity contents of HPDCM samples, Group 5 and Group 4 samples exhibited the lowest and the highest porosity contents, respectively. On the other hand, pore size distribution of samples was not proportional to their porosity contents. The size of the pores in Group 1, 2, and 5 samples were more or less the same with an average pore size around ~3-5 μm. Relatively larger pores were observed in Group 3 and Group 4 samples. Although the Group 3 sample possessed relatively low amount of porosity with respect to Group 4 sample, it had pores as large as 100 μm, while the maximum pore size in Group 4 samples was around 20 μm.

Figure 3 shows x-ray tomography images of the samples. Similar to microstructural examination, all of the HPDCM samples displayed pores as shown by arrows. Group 3 samples exhibited the largest pore size among the HPDCM as determined from the microstructural examination (Fig. 2c). On the other hand, no detectable porosity was observed in x-ray tomography images of CCM samples. Presence of excessively larger pores in Group 3 samples was attributed to "jetting" phenomenon caused by high gate (nozzle inlet) speed, high pressure, and low temperature settings. The lowest gate speed, which fills the mold without solidification, should be selected to eliminate the jetting. Although the inlet velocity less than 30 m/s can be used for parts with thicknesses above 5 mm, these velocities may also lead to an increase in the amount of porosity caused by shrinkage. In the present study, the velocity exceeding 50 m/s (Table 2, 60 m/s) increased the pore size of the samples as well due to larger amounts of trapped gasses in the casting cavity which caused vortex marks on the sample surface due to turbulent flow. As shown in Fig. 2(e), lowering the in-mold pressure and gate speed with an increased casting temperature (Group-5 parameters in Table 2) yielded samples with lower porosity and small micro pores.

SEM images showing the surface morphologies of as-cast samples are presented in Fig. 4. Although all of the samples displayed some micro pores on their surface left from casting, surface pores in Group 2 and Group 3 samples were more evident. The largest surface pores, as large as 400 μm, was detected in Group 3 samples.

As well as the surface condition and presence of porosity, the underlying microstructure is also crucial since it determines the properties of materials (hardness, strength, resistivity, etc.), thereby influencing the machining performance. Figure 5 shows the microstructures of as-cast samples. All of the HPDCM samples (Group 1-5 samples) contained dendritic α-phase surrounded by $Mg_{17}Al_{12}$ phase as shown black and red arrows, respectively, in Fig. 5. Compared to CCM samples, finer microstructure was obtained in HPDCM samples possibly due to faster cooling rate encountered in HPDCM. On the other hand, utilizing relatively slower cooling rate in CCM resulted in coarser microstructure as shown in Fig. 5(f). Additionally, slower cooling rate also changed the types of phases present in the microstructure. Similar to HPDCM samples, the microstructure of CCM samples contained dendritic α-phase and $Mg_{17}Al_{12}$ phase. However, one more phase mixture, called eutectic phase mixture (composed of α and $Mg_{17}Al_{12}$ phases), was also detected in CCM samples in the lamellar morphology as shown by blue arrows in Fig. 5(f).

3.2 Properties of as-cast samples

The properties of as-cast samples are presented in Table 5. The strength and hardness values of samples were previously obtained in the works of one of the authors of the present study Ref 11, 12. Although HPDCM samples contained some amount of micro porosity, they displayed higher hardness and tensile strength values compared to CCM samples possibly due to their finer microstructures. However, among the HPDCM samples, Group 3 samples exhibited the lowest hardness and tensile strength values close to those of CCM samples mainly due to

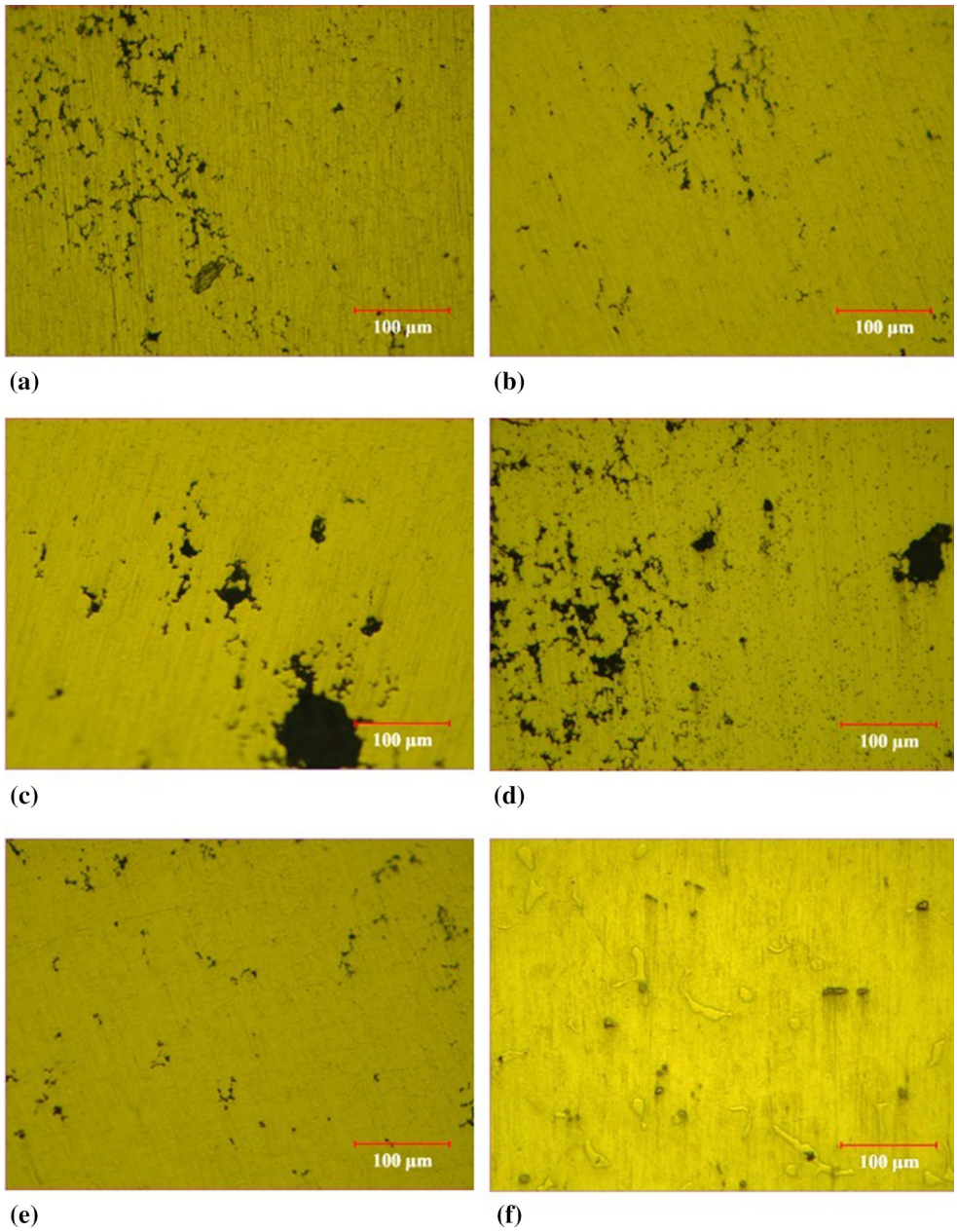

Figure 2. Optical microscope image of polished cross sections of as-cast samples, (a) Group 1, (b) Group 2, (c) Group 3, (d) Group 4, (e) Group 5, (f) CCM samples

Table 4. Total porosity of the HPDCM (Group 1-5) and CCM samples

Sample	Group 1	Group 2	Group 3	Group 4	Group 5	CCM
Total porosity (%)	3.8±1.5	2.8 ± 0.7	3.0±0.3	4.8 ± 0.5	2.6 ± 0.4	0.3 ± 0.2

presence of larger pores and flaws, which acted as crack nucleation sites. On the other hand, the measured electrical resistivities of HPDCM and CCM samples were observed to be different. HPDCM samples' electrical resistivity values were more or less the same mainly due to similar fine microstructure obtained in all Groups of HPDCM samples. However, electrical resistivity of CCM was to be around ∼165 nΩ.m, which was slightly higher than that of HPDCM samples (∼160 nΩ.m). Interestingly, CCM samples with coarser dendritic phases displayed higher resistivity. It is known that higher interface area between the phases increases the resistivity due to increased scattering sites for electrons. The high resistivity in CCM samples was attributed to formation of fine lamellar eutectic mixture (Fig. 5f), which increased the interfacial area in the material.

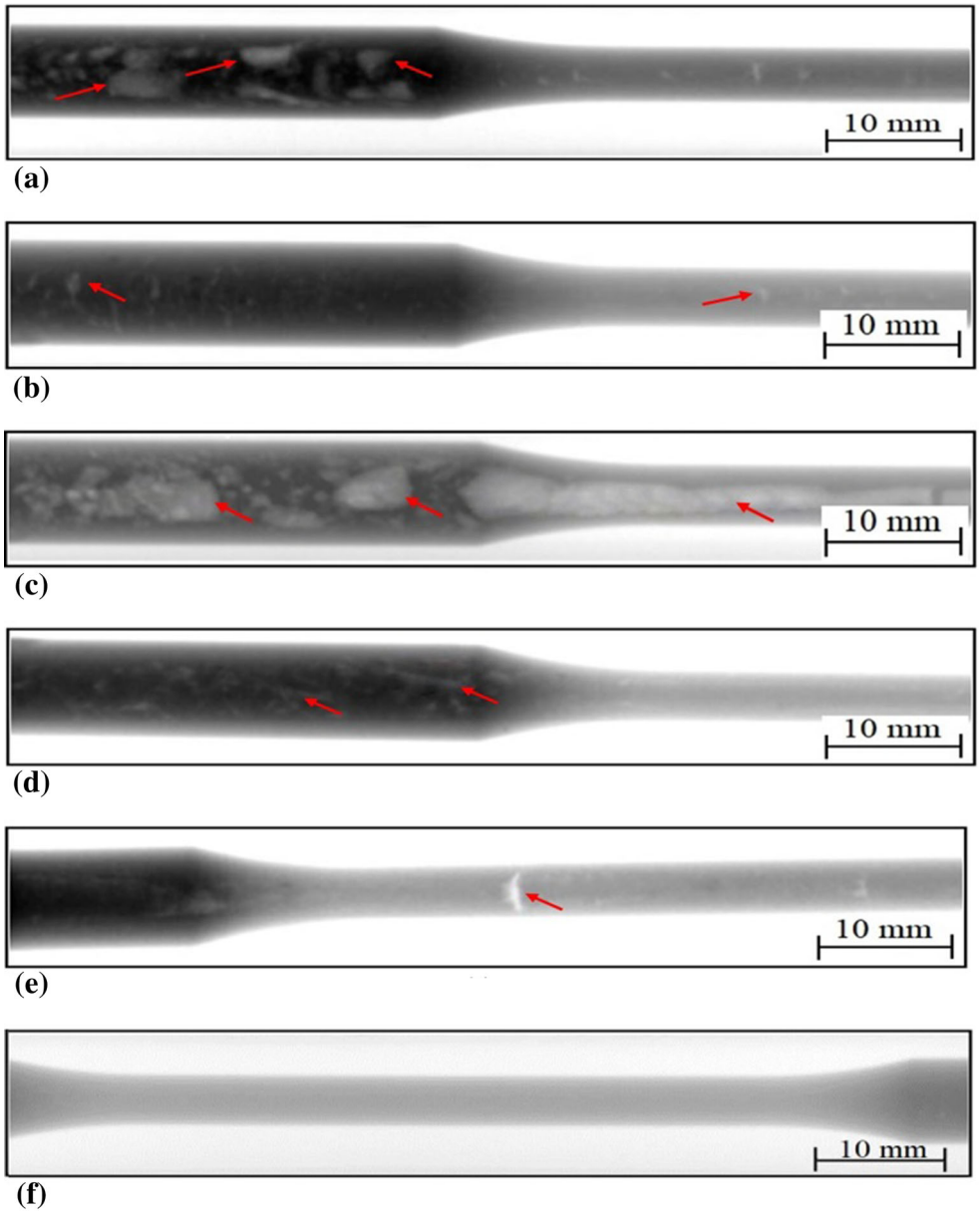

Figure 3. X-ray tomography images of samples, (a) Group 1, (b) Group 2, (c) Group 3, (d) Group 4, (e) Group 5, (f) CCM samples

3.3 Machining of Samples

Figure 6 and 7 displays the change of I for different WEDM parameters at two different V_w values. The highest I value for both HPDCM and CCM samples were observed at the HPL setting for two V_w values, namely, 4 m/min and 6 m/min. For the same power level, although there was no significant change in I value for HPDCM samples, comparatively higher I value was observed for CCM samples. However, the MR values of CCM samples were lower than that of HPDCM samples for both V_w settings (Fig. 8 and 9). This finding was consistent with the variations of I (Fig. 6 and 7) since the machine control unit increases I to increase the MR. However, the increase of I by means of the control unit during WEDM of CCM samples couldn't increase the MR values proportionally. The machine control unit also limits the I value not to increase the cutting speed (i.e., the MR) further since high cutting speed may cause wire breakage due to excessive tensioning of the wire during forward movement. The lower MR values of CCM samples than HPDCM specimens were attributed to slightly higher electrical resistivity (i.e., low electrical conductivity) (Table 5) and their lower amount of porosities (Table 4).

In this experimental study, one more observation is worth to mention that the much higher MR value was measured in Group 3 samples (Fig. 8 and 9) among the HPDCM samples in all power levels despite the similar I value. The higher MR value in Group 3 samples was attributed to the reduction of net sample thickness to be cut due to existence of the comparatively larger pores and cavities compared to other samples (Fig. 2c, 3c and 4c). The other groups of HPDCM samples revealed similar MR values possibly due to their similar microstructure and pores size in addition to same resistivity values.

Figure 8 and 9 also revealed the positive impact of increasing V_w on MR with higher MR values at higher V_w values. Increasing V_w provides existence of the less worn wire,

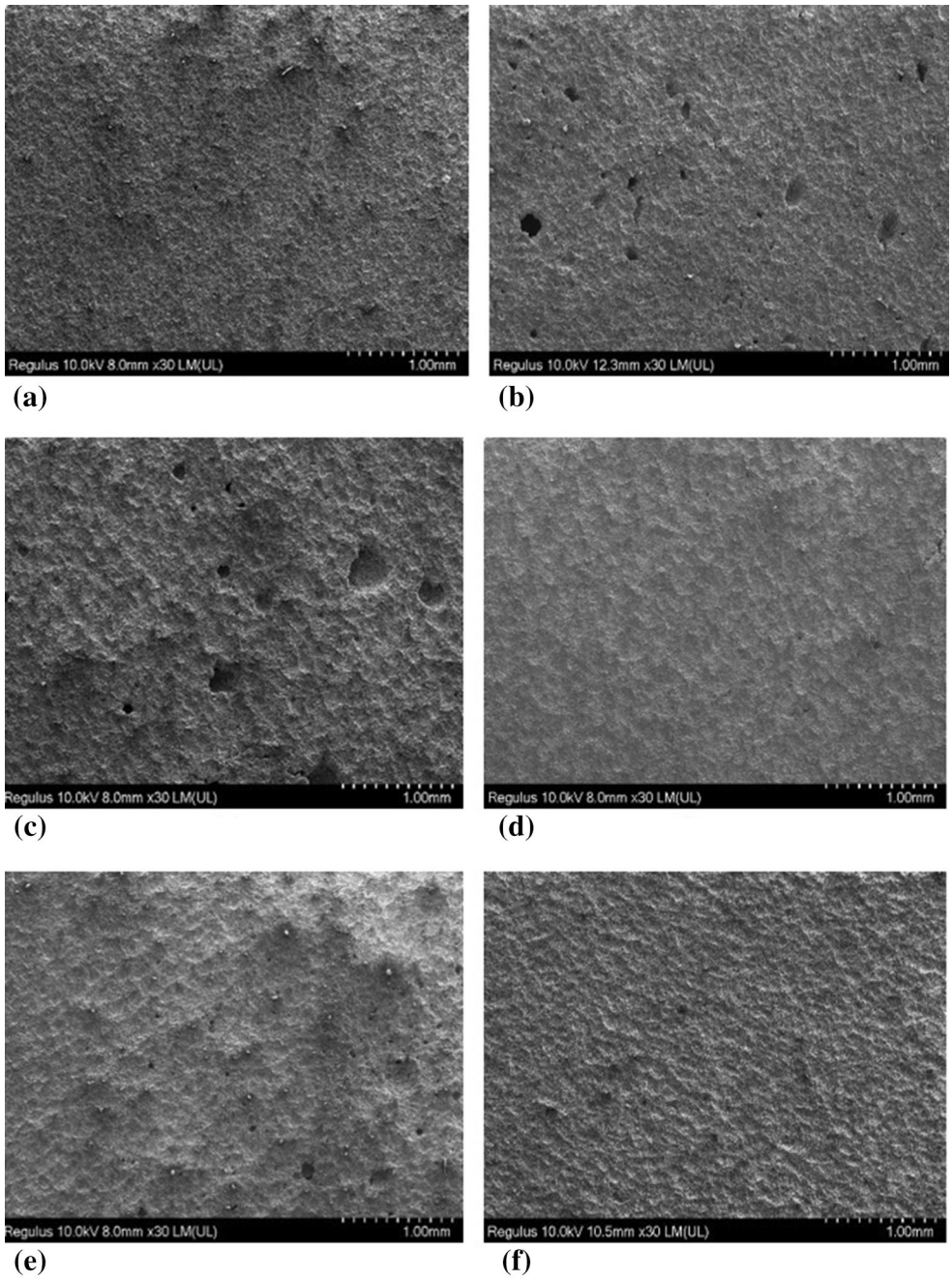

Figure 4. Surface SEM images of as-cast samples (a) Group 1, (b) Group 2, (c) Group 3, (d) Group 4, (e) Group 5, (f) CCM samples

which can carry higher current to generate more effective discharge pulses as well as resist higher spark push forces without breakage, in the machining gap.

Utilizing different WEDM parameters (LPL, MPL, and HPL) also changed R_a values of samples. The highest R_a values were experienced at the HPL settings (Fig. 10 and 11). This is attributed to the formation of high-energy discharges in the machining gap forming wider and deeper craters on the surface (rough surface). The high current application to the CCM samples by the control unit of the machine (Fig. 6 and 7) yielded the roughest sample surfaces (the highest R_a values) (Fig. 10 and 11). Within the WEDM settings all of the HPDCM samples displayed similar R_a values mainly due to their similar microstructures and the I values. The R_a values seen in Fig. 10 and 11 were in agreement with the I values in Fig. 6 and 7 since the surface roughness is proportional with the applied I to the samples (higher energy discharge pulses form deeper craters on the surface yielding poor surface quality).

In WEDM process, the electric discharges (sparks) melt and evaporate small amount of material on the surface by forming craters. The examination of the SEM images (Fig. 12) revealed the formation of micro-cracks on the surface due to rapid solidification of molten material by means of dielectric fluid. No evident differences between the SEM images of the Groups 1-6 regarding the micro-crack formation density, micro-crack shapes and orientations, and surface textures were observed.

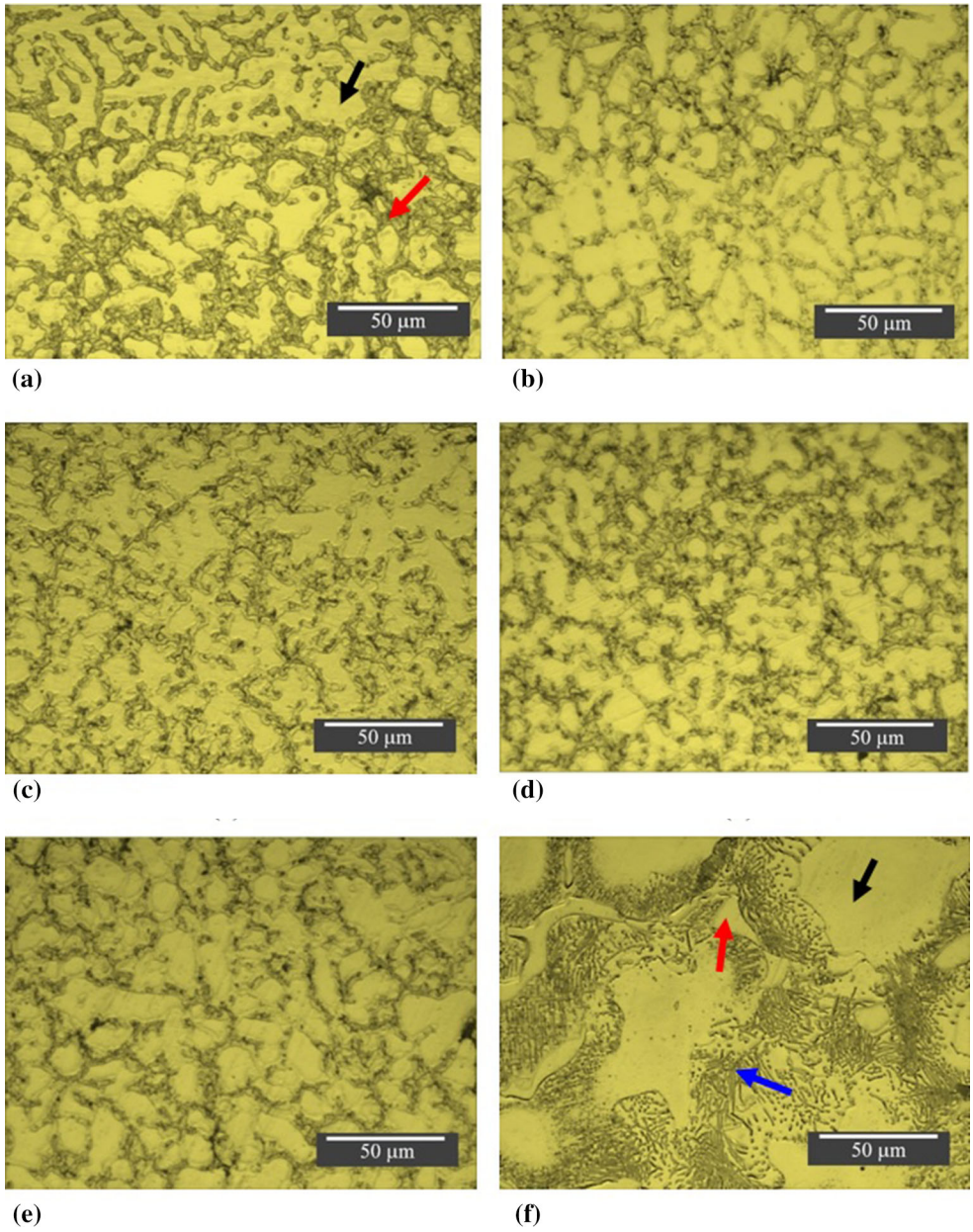

Figure 5. Optical microscope image of etched cross sections of as-cast samples, (a) Group 1, (b) Group 2, (c) Group 3, (d) Group 4, (e) Group 5, (f) CCM samples

Table 5. Measured properties of as-cast HPDCM (Group 1-5) and CCM samples

Sample	Tensile strength, MPa	Brinell hardness, BHN	Electrical resistivity, nΩ.m
Group 1	201	70.2	161
Group 2	198	69.4	161
Group 3	168	64	159
Group 4	221	84.3	160
Group 5	214	77.6	160
CCM	169	62	165

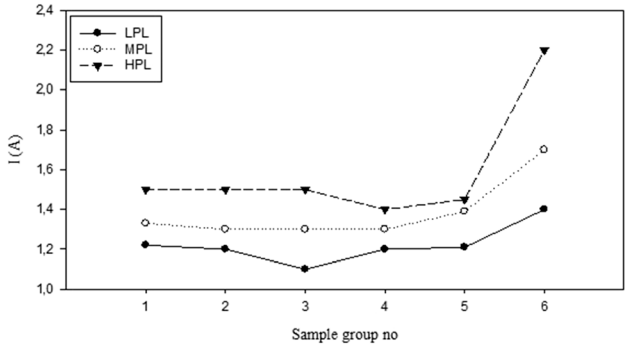

Figure 6. Variations of I for HPL, MPL and LPL settings (V_w = 4 m/min)

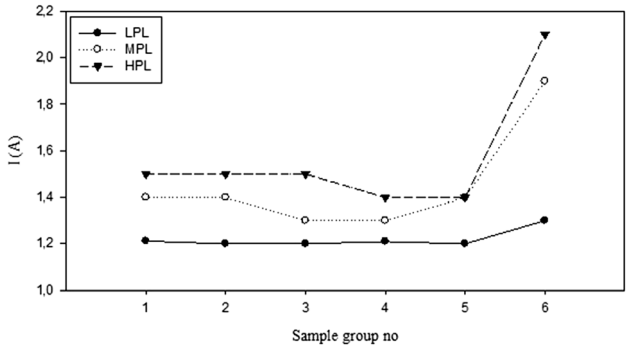

Figure 7. Variations of I for HPL, MPL and LPL settings (V_w = 6 m/min)

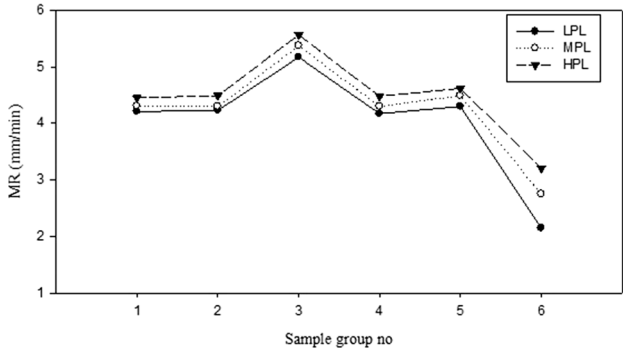

Figure 8. Variations of MR with HPL, MPL and LPL settings (V_w = 4 m/min)

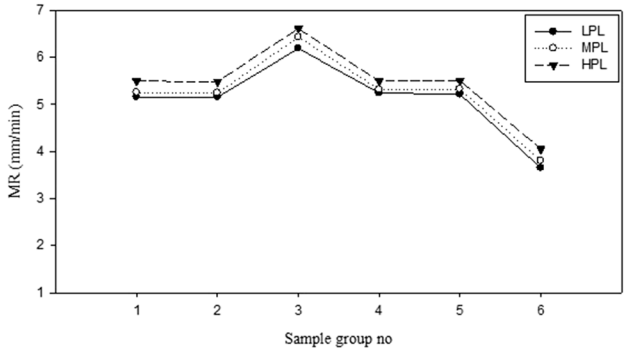

Figure 9. Variations of MR with HPL, MPL and LPL settings (V_w = 6 m/min)

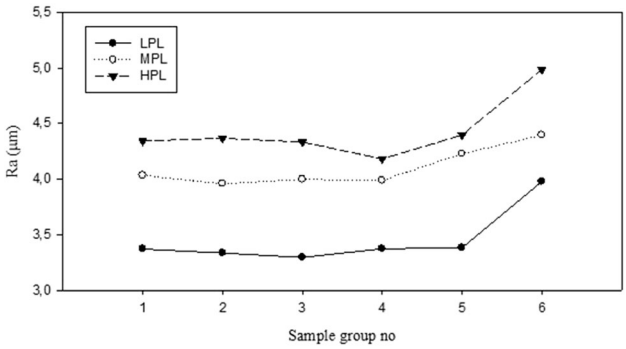

Figure 10. Variation of R_a with HPL, MPL, and LPL settings (V_w = 4 m/min)

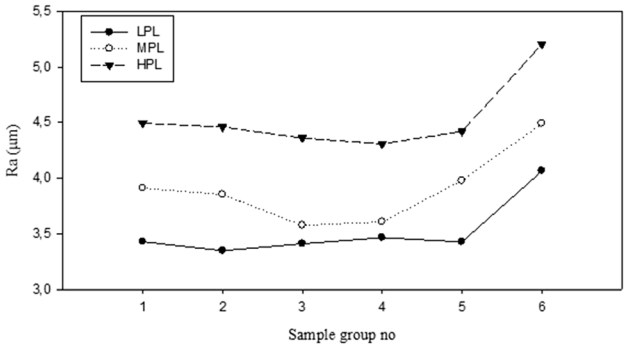

Figure 11. Variation of R_a with HPL, MPL, and LPL settings (V_w = 6 m/min)

4. Conclusion

In this study, the WEDM machinability and machined surface characteristics of AZ91 alloy were studied by considering the effect of underlying microstructure together with the electrical resistivity of the alloys produced by HPDCM and CCM. Following conclusions have been drawn regarding the effect of casting technique on microstructure, electrical resistivity, and machining performance of the alloys:

- HPDCM samples possessed comparatively higher strength and hardness because of their finer microstructures due to faster cooling rate.
- The density of HPDCM samples was influenced from the casting variables such that larger pores appeared in the microstructure when higher gate (nozzle inlet) speed and pressure were utilized together with low temperature settings.
- Relatively slow cooling of CCM samples resulted in denser samples and formation of coarser α-dendrites and $Mg_{17}Al_{12}$ phase together with fine eutectic mixture, which was thought to be the reason of slightly higher resistivity.
- For all types of samples, higher I and MR values were obtained for HPL settings. Although I value was not influenced from the wire speed remarkably, considerable increase was observed in MR value when wire speed was increased at any setting configurations (LPL, MPL and HPL).

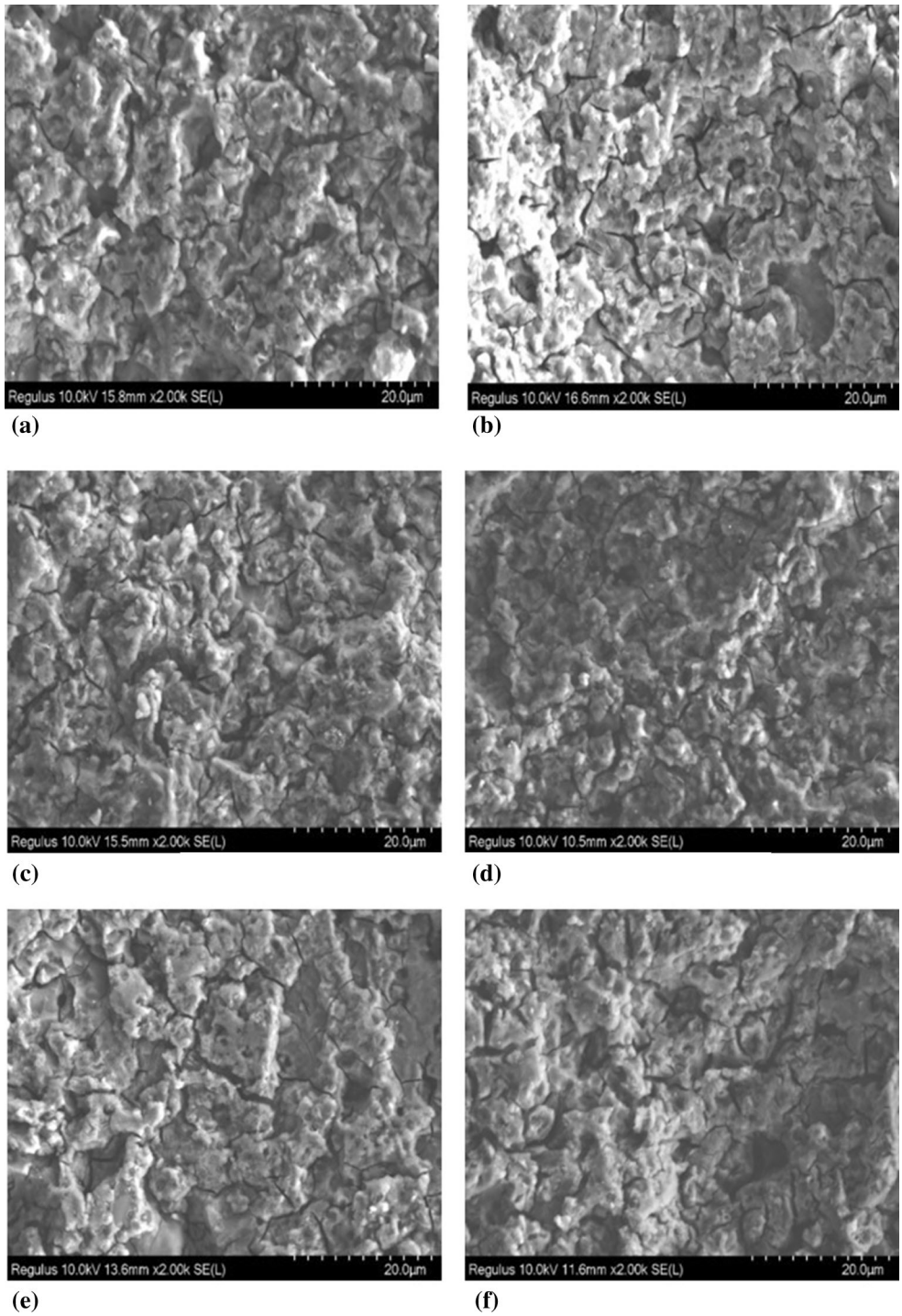

Figure 12. SEM images of HPDCM and CCM samples after machining (at MPL machining parameters). (a) Group 1, (b) Group 2, (c) Group 3, (d) Group 4, (e) Group 5, (f) CCM samples

- For the same power level, due to their denser structures and slightly higher resistivity, CCM samples exhibited comparatively lower MR values which were accompanied higher I values automatically increased by the control unit of the machine tool.
- Regardless of the setting configurations, measured I values were similar for all HPDCM samples due to their similar microstructures and porosity contents; however, MR value of Group 3 samples was higher for any types of settings and wire speeds mainly due to presence of larger pores, which made the effective cross-sectional area to be cut smaller.
- All samples machined at HPL settings displayed higher surface roughness due to formation of wider and deeper craters because of high-energy discharges formed in the machining gap. Despite similar roughness values of HPDCM samples having similar underlying microstructure, CCM samples showed higher roughness values

mainly due to higher machining current automatically adjusted by the control unit.
- In all samples, WEDM resulted in formation of craters and micro-cracks on the surfaces of samples due to melting, evaporation, and rapid solidification of molten material.

Acknowledgment

The production of HPDCM samples was carried out under the scope of the MMF.A3.17.003 coded Scientific Research Project (BAP). The authors would like to thank Kırşehir Ahi Evran University (Turkey) BAP Division.

References

1. M. M. Avedesian and H. Baker, ASM specialty handbook: Magnesium and magnesium alloys, ASM International, USA, 1999
2. C. Blawert, N. Hort and K.U. Kainer, Automotive applications of magnesium and its alloys, *Trans.- Indian Inst. Metals*, 2004, **57**(4), p 397-408
3. M.V. Segal, Materials processing by simple shear, *Mater. Sci. Eng., A*, 1995, **197**(2), p p157-164
4. K. Máthis, G. Jenő and N.H. Nam, Microstructure and mechanical behavior of AZ91 Mg alloy processed by equal channel angular pressing, *J. Alloy. Compd.*, 2005, **394**(1-2), p 194-199
5. E. Koç, M. Ünal, Y. Türen and E. Candan, Effect of TIN on Casting and Mechanical Properties of AZ91 Magnesium Alloy, *5. International Advanced Technologies Symposium (IATS'09),* 13–15 May 2009, Karabük, Turkey
6. A.S.J. Al-Zubaydi, A.P. Zhilyaev, S.C. Wang and P.A.S. Reed, Superplastic behaviour of AZ91 magnesium alloy processed by high-pressure torsion, *Mater. Sci. Eng., A*, 2015, **637**, p 1-11
7. Y. Türen, Effect of Sn addition on microstructure, mechanical and casting properties of AZ91 alloy, *Mater. Des.*, 2013, **49**, p 1009-1015
8. E. Uhlmann, S. Piltz and D. Oberschmidt, Machining of micro rotational parts by wire electrical discharge grinding, *Prod. Eng. Res. Devel.*, 2008, **2**(3), p 227-233
9. F. Klocke, M. Schwade, A. Klink and A. Kopp, EDM machining capabilities of magnesium (Mg) alloy WE43 for medical applications, *Procedia Eng.*, 2011, **19**, p 190-195
10. A. Mostafapor and H. Vahedi, Wire electrical discharge machining of AZ91 magnesium alloy; investigation of effect of process input parameters on performance characteristics, *Eng. Res. Express*, 2019, **1**(1), p 015005
11. U. Köklü, S. Morkavuk and L. Urtekin, Effects of the drill flute number on drilling of a casted AZ91 magnesium alloy, *Mater. Testing*, 2019, **61**(3), p 260-266
12. Ş Yazman, U. Köklü, L. Urtekin, S. Morkavuk and L. Gemi, Experimental study on the effects of cold chamber die casting parameters on high-speed drilling machinability of casted AZ91 alloy, *J. Manuf. Process.*, 2020, **57**, p 136-152